White-noise susceptibility and critical slowing in neurons near spiking threshold

D. A. Steyn-Ross,[1,*] Moira L. Steyn-Ross,[1] M. T. Wilson,[1] and J. W. Sleigh[2]
[1]*Applied Physics, Department of Engineering, Private Bag 3105, University of Waikato, Hamilton 3240, New Zealand*
[2]*Department of Anaesthetics, Waikato Hospital, Hamilton, New Zealand*

(Received 8 September 2005; revised manuscript received 12 September 2006; published 30 November 2006)

We present mathematical and simulation analyses of the below-threshold noisy response of two biophysically motivated models for excitable membrane due to H. R. Wilson: a squid axon ("resonator") and a human cortical neuron ("integrator"). When stimulated with a low-intensity white noise superimposed on a dc control current, both membrane types generate voltage fluctuations that exhibit *critical slowing down*—that is, the voltage responsiveness to noisy input currents grows in amplitude while slowing in frequency—as the membrane approaches spiking threshold from below. We define *threshold* unambiguously as that dc current that renders a zero real eigenvalue for the Jacobian matrix for the integrator neuron, and, for the resonator neuron, as the dc current that gives a complex eigenvalue pair whose real part is zero. Using a linear Ornstein-Uhlenbeck analysis, we give exact small-noise expressions for the variance, power spectrum, and correlation function of the voltage fluctuations, and we derive the scaling laws for the divergence of susceptibility and correlation times for approach to threshold. We compare these predictions with numerical simulations of the nonlinear stochastic equations, and demonstrate that, provided the white-noise perturbations are kept sufficiently small, the linearized theory works well. These predictions should be testable in the laboratory using a current-clamped cell configuration. If confirmed, then the proximity of a neuron to its spike-transition point can be judged by measuring its subthreshold susceptibility to white-noise stimulation. We postulate that such temporally correlated fluctuations could provide a means of subthreshold signaling via gap-junction connections with neighboring neurons.

DOI: 10.1103/PhysRevE.74.051920 PACS number(s): 87.19.La, 05.10.Gg, 05.70.Fh, 87.17.Aa

I. INTRODUCTION

A. Neural communication

It is generally taken as axiomatic that a neuron encodes and transmits information about its inputs by generating one or more action potential "spikes" that propagate along its axon to synaptically connected receiving neurons. The fact that a biological *in vivo* neuron must process its input signals in the presence of a continuous wash of noise immediately raises the question: How is the neuron able to encode information reliably? This reliability problem has attracted much attention [1–4] and has lead to the counterintuitive finding that, in nonlinear systems, moderate levels of noise can both improve the fidelity of signal transmission (described as "stochastic resonance") [5–8] and enhance the periodicity of an oscillatory component of the system's behavior ("stochastic coherence") [9,10].

The underlying assumption is that only the spiking neurons transmit information, and that subthreshold neurons—neurons that have not yet received sufficient excitation to cross the threshold for action potential generation—play no active role in interneuron communication. Consequently, most modeling investigations of Hodgkin-Huxley neurons have focused on the generation and propagation of the action potential. However, the discovery that adjacent cortical neurons can form intimate bidirectional electrical connections, known as *electrotonic* or *gap junctions* [11,12], suggests that, in addition to the well-known neurochemical synaptic junctions, cortical neurons also have access to electrically diffusive channels that permit subthreshold communication between cells, evidenced as enhanced neuronal synchronization between cell populations [13]. Gap junctions connect interneuron dendrites to other dendrites, as well as to axons and to glial cells [13,14]; within a given cortical hemisphere, there is no apparent limit to the extent of interneuron gap junction networks [15,16].

In view of the apparent ubiquity of gap-junction communications within the cortex, we are motivated to ask the question: How might a noise-driven subthreshold neuron signal to its neighbors that it is about to generate a spike? Using a linearized stochastic analysis, we will demonstrate that a near-threshold neuron exhibits output voltage fluctuations that are "critically slowed" yet exquisitely susceptible to fluctuations in the input current—that is, the voltage fluctuations become increasingly correlated in time and divergent in amplitude as threshold is approached from below.

Our analysis of neuron dynamics is based on a linear perturbation expansion about the neuron's near-threshold stationary state. This is a standard approach which is well-described by Rinzel and Ermentrout [17], and in Strogatz' [18] textbook. Also well-known is the fact that neuron response near a bifurcation point becomes critically slowed; this is a generic result that applies irrespective of whether the bifurcation is of Hopf or saddle-node type [3,17–19], and therefore is expected behavior for the two H. R. Wilson neuron models we analyze here. However, these previous discussions of critical slowing in neuron models seem to lack any quantitative treatment of the interaction between the eigenvalue structure of the subthreshold neuron and the noisy environment in which all biological neurons must function. By combining pertinent stochastic calculus results (derived

*URL: phys.waikato.ac.nz/cortex. Electronic address: asr@waikato.ac.nz

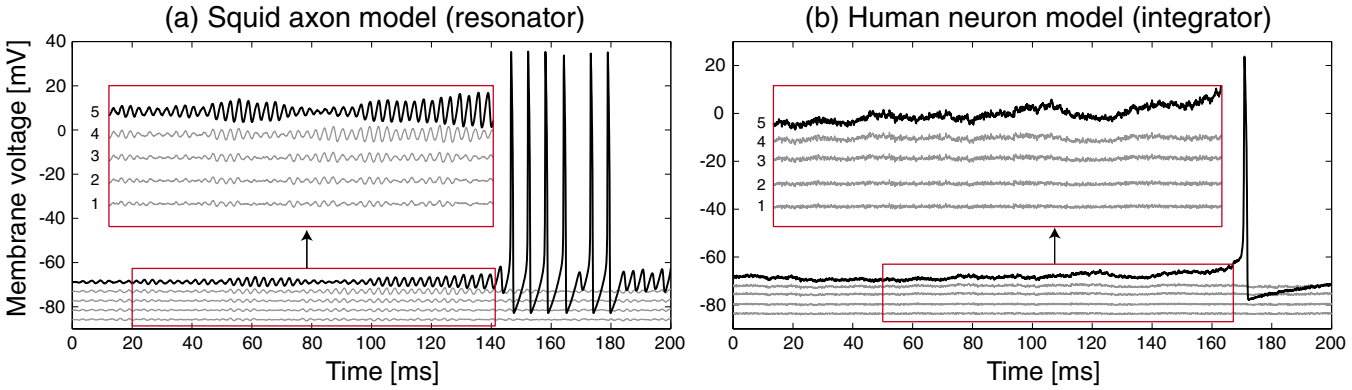

FIG. 1. (Color online) Stochastic simulations for the Wilson models for (a) squid axon and (b) human cortical neuron. Framed insets show detail of the subthreshold voltage fluctuations prior to spike onset. (a) Numbered from bottom to top, the five squid stimulation currents are $I_{dc}=0$, 2, 4, 6, and 7.7 $\mu A/cm^2$. (To improve visibility, the squid traces have been displaced vertically by $(4m-20)$ mV where $m=1,\ldots,5$ is the curve number.) (b) Cortical neuron stimulation currents are (bottom to top) $I_{dc}=-100$, -40, 0, +16, and +21.4752 $\mu A/cm^2$. Integration algorithm is semi-implicit Euler-trapezium [39] with time step $\Delta t=0.005$ ms. To aid intercomparison of the traces, each of the five simulation runs within a given figure used the same sequence of 40 000 Gaussian-distributed random-number pairs to generate the $(\xi_1(t),\xi_2(t))$ white-noise perturbations.

by Gardiner [20] for the multivariate Ornstein-Uhlenbeck process) with our near-threshold eigenvalue analysis, we are able to derive exact predictions for spectral and temporal fluctuations in neuron voltage that are valid in the small-noise limit.

In this paper we present a theoretical analysis of the white-noise-induced voltage fluctuations in an excitable membrane near threshold, and we derive scaling laws for the correlation time and susceptibility as the membrane approaches spiking threshold.

B. Resonator and integrator membranes

All biophysically realistic models for excitable membranes can be classified according to the nature of the onset of their spiking behavior. For the squid axon and for auditory nerve cells, action potential oscillations emerge at a nonzero frequency when an injected dc stimulus current exceeds a threshold value; such membranes are classified as being type-II. In contrast, for type-I membranes (e.g., human cortical neurons) spike oscillations emerge at zero frequency as the current stimulus crosses threshold. That is, the firing frequency in a type-I neuron can be arbitrarily slow.

This historical taxonomy of neuron types is due to Hodgkin [21]. A more evocative naming scheme due to Izhikevich [19] highlights the very different dynamical responses of the two membranes; thus a type-II neuron is called a *resonator*, and a type-I neuron is an *integrator*. (The

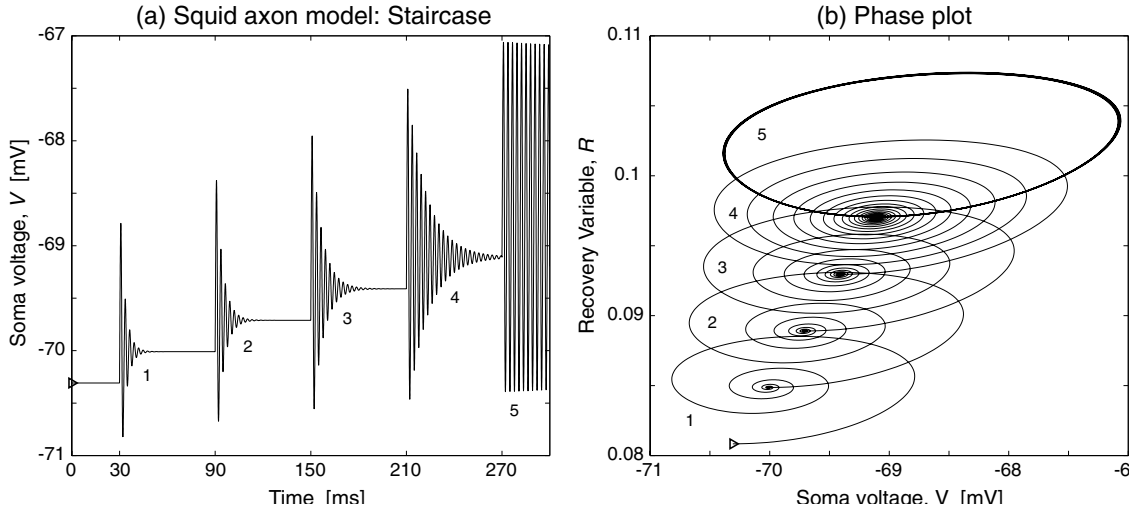

FIG. 2. Subthreshold impulse response for the Wilson model of a squid-axon membrane (a "resonator") driven by a staircase-shaped I_{dc} stimulus current that follows an upwards stair-step pattern towards firing threshold. (a) V-vs-t time series for membrane voltage. (b) R-vs-V voltage-recovery phase-plot corresponding to the time series in (a). The initial current at time $t=0$ is $I_{dc}=-4.0$ $\mu A/cm^2$; the current is stepped upwards at $t=30$ ms, held steady for 60- ms, then stepped again at 60-ms intervals. Each of the five current increments is of magnitude $\Delta I_{dc}=2.33$ $\mu A/cm^2$. The final current, imposed at $t=270$ ms, is $I_{dc}=7.65$ $\mu A/cm^2$, close to the spiking threshold $I_{dc}^{crit}\approx 7.77327$ $\mu A/cm^2$. Successive oscillatory impulse responses become increasingly long-lived as the I_{dc} stimulus current approaches threshold. (Integration was by semi-implicit Euler with time step $\Delta t=0.02$ ms.)

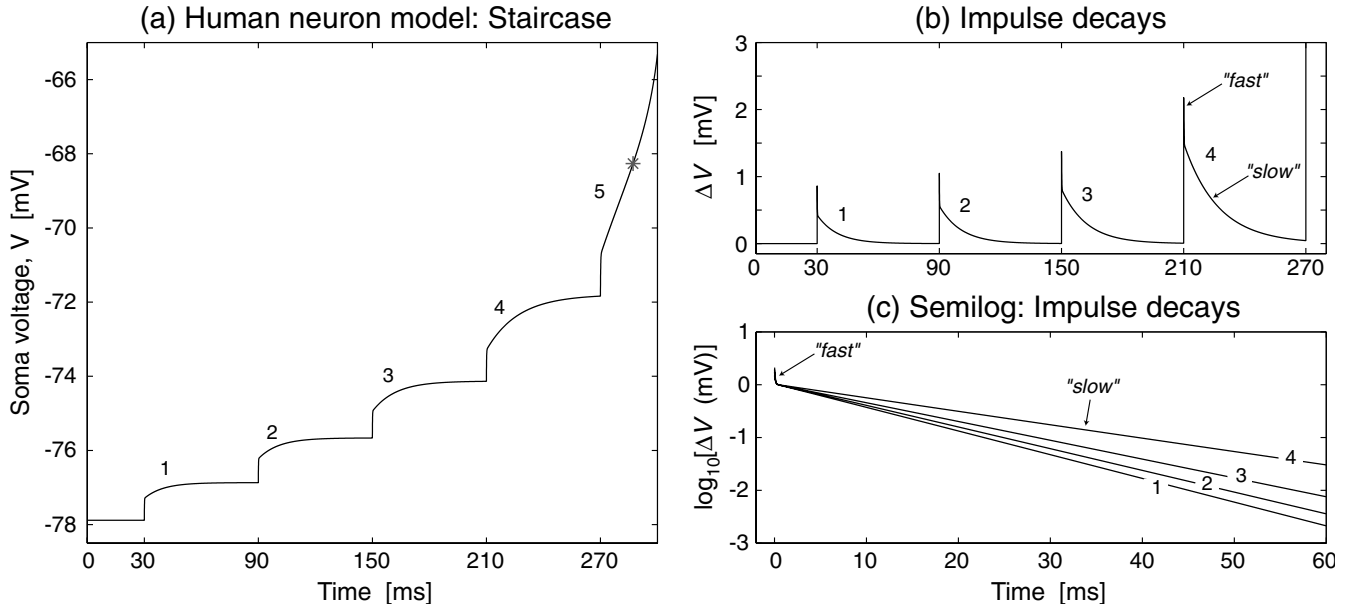

FIG. 3. Subthreshold impulse response for the Wilson model of a human cortical neuron (an "integrator") driven by a staircase-shaped I_{dc} stimulus current that steps upwards, at 60-ms intervals, towards firing threshold. (a) V-vs-t time series for membrane voltage; the asterisk (in red) marks the point at which the neuron voltage crosses its threshold potential $V^{crit} \approx -68.2653$ mV—the membrane is about to generate a fully formed action potential (not shown). (b) ΔV-vs-t time series for the decay of membrane voltage back to steady state; obtained by subtracting the time-series graph of (a) from the theoretical staircase distribution of equilibrium voltages computed for each level of stimulation current: $\Delta V(t) = V^{o}(I_{dc}) - V(t)$. (c) The four decays shown in (b), replotted to a common time scale that is reset to zero with each step-change in current, drawn on a logarithmic vertical scale. There are five increments in current, each of size $\Delta I_{dc} = 9.2\ \mu A/cm^2$. The initial current $I_{dc}(t=0) = -20.0\ \mu A/cm^2$; the final current is $I_{dc} = 26.0\ \mu A/cm^2$, well above the spiking threshold $I_{dc}^{crit} \approx 21.4752\ \mu A/cm^2$. Note that the decay to steady state occurs on two time scales, labeled "fast" and "slow" in graphs (b) and (c). The "slow" evolution becomes ever slower as the dc stimulus current approaches spiking threshold. (Integration time step: $\Delta t = 0.02$ ms.)

aptness of these names will become apparent later in the paper—for a preview, see Figs. 1–3.)

The distinction between the two membrane types has been explored by Rinzel and Ermentrout [17] using linear stability theory to explore the subthreshold behavior, and phase-plane analysis to trace the nonlinear limit-cycle dynamics that emerge above threshold. As the stimulus current is increased towards threshold, the (real part of the) dominant eigenvalue approaches zero from below. With further increase in stimulus, the eigenvalue changes sign and the resting steady state becomes unstable—the nerve cell abruptly changes state from quiescence to active firing. For both types of cell, the imaginary part of the eigenvalue near threshold is indicative of the frequency of the spike oscillations that are about to emerge. Thus for a subthreshold resonator cell, the eigenvalues are complex, implying the abrupt emergence of a nonzero spike-oscillation frequency, while for an integrator both eigenvalues are purely real, implying a zero-frequency firing rate.

Real neurons *in vivo* are exposed to a continuous wash of noise arising from a range of sources such as thermal fluctuations and spontaneous release of neurotransmitter quanta at presynaptic vesicles [22,23]. This noisy background will tend to cause uncertainty in the timing of spike events, but, in the subthreshold neuron, these small random perturbations could be useful: not only would they enable the neuron to explore its nearby state-space, but the neuron's responsiveness to these ever-present Brownian jostlings might provide a subthreshold means of communication to neighboring neurons. This possibility motivates us to ask the question: Can a quiescent cell's nearness to transition be determined from an examination of its noise-evoked fluctuations? We will find that—for both types of neuron—the answer is yes: the approach to transition is predicted to exhibit a phase-transition-like *critical slowing down* of the temporal and spectral characteristics of the fluctuation responsiveness. By applying Ornstein-Uhlenbeck theory to Wilson's [24] two-variable resonator and integrator neuron models, we are able to write down exact expressions for the fluctuation variance, spectral distribution, and time-correlation functions. As the cell nears transition, the linear theory predicts that these quantities will exhibit divergences that herald the imminent and abrupt phase changeover from small-scale subthreshold linear stochastics to gross-scale nonlinear spiking dynamics. We verify these near-threshold predictions with stochastic numerical simulations of the full nonlinear equations.

Although multivariate Ornstein-Uhlenbeck theory has been used to quantify phase transition behavior in cortical models for induction of anesthesia [25–28], and within the cycles of natural sleep [29–31], to our knowledge this is the first time this method has been applied to understanding the nonlinear amplification and susceptibility properties of near-threshold excitable membranes.

The plan of the paper is as follows. In Sec. II we present the Wilson models for squid axon and human cortical neuron. We investigate, via simulation, how the responsiveness

of these excitable membranes varies on approach to spiking threshold when driven (a) by white noise riding on a dc current, and (b) by a noise-free current staircase, then give a preliminary explanation in terms of their steady states and eigenvalue structure. Section III maps the Wilson equations to an Ornstein-Uhlenbeck model, then applies well-established stochastic calculus results to give expressions for the variance, correlation time, and power spectral density of the membrane fluctuations, and to deduce the near-threshold scaling laws for the slow time-scale and white-noise susceptibility. Section IV details a series of numerical experiments that test the theoretical predictions. Finally, in Sec. V, we describe briefly a plausible laboratory experiment, and we speculate on the possible biological significance of critical slowing in near-threshold neurons.

II. MODEL EQUATIONS

This paper focuses on the subthreshold behavior of a pair of reduced, but biophysically realistic, voltage-recovery spiking models for excitable membrane presented in 1999 by Wilson [24]. A brief provenance of the Wilson equations follows.

In 1985, Rinzel [32] had realized that the fourth-order Hodgkin-Huxley (HH) [33] equations describing action-potential generation in the squid giant axon could be simplified to second order by (a) treating Na^+ channel activation as a "fast," rapidly equilibrating variable, and (b) combining the two "slow" variables (K^+ channel activation and Na^+ channel inactivation) into a single *recovery* variable R. These reduced equations contain most of the biophysical content of the HH equations, and so remain difficult to analyze because of the transcendental character of several of their terms. Earlier modeling due to FitzHugh [34] and Nagumo [35] had focused on mathematical simplicity. The FitzHugh-Nagumo equations retain the essential cubic nonlinearity for spike generation, but discard most of the physiological details of the HH equations, such as adherence to Ohm's law and explicit reference to the Na^+ and K^+ reversal potentials. Wilson [24] describes his alternative approach as

> "…a more accurate approximation to the Hodgkin-Huxley equations that rectifies the shortcomings of the FitzHugh-Nagumo equations while retaining their mathematical tractability."

The Wilson equations acquire their simplicity by replacing Rinzel's transcendental dependencies by *polynomial* fits to the Rinzel isoclines. With a minor change to the form of the polynomial fits, the Wilson equations are capable of simulating action potential formation in both squid axon (resonator, type II) and in cortical neuron (integrator, type I) nerve membranes.

It is for these reasons—versatility, biophysical plausibility, and mathematical tractability—that we selected the Wilson equations as the target for our stochastic analysis. Despite this particular choice, we believe that the conclusions we reach regarding white-noise susceptibility and critical-slowing behaviors in the subthreshold nerve are not unique to this model, but rather are *general properties* shared by all excitable membranes.

The Wilson equations are expressed in terms of ionic and injected current flowing through the lipid membrane capacitance to establish a membrane voltage, coupled to a slow recovery variable that responds to the membrane voltage. We bring stochasticity to the noise-free Wilson model by adding white-noise perturbations to the current and to the recovery.

The noise-perturbed Wilson equations read

$$C\frac{dV}{dt} = -g_{\mathrm{Na}}(V)(V-E_{\mathrm{Na}}) - g_{\mathrm{K}}R(V-E_{\mathrm{K}}) + I_{\mathrm{dc}} + \sigma_I\xi_1(t), \tag{1a}$$

$$\tau_R\frac{dR}{dt} = -R + G(V) + \sigma_R\xi_2(t). \tag{1b}$$

Here, V is the membrane voltage and C is the membrane capacitance per unit area; R is a (dimensionless) recovery variable that represents the combined action of K^+ channel opening and Na^+ channel closing; and τ is the time-constant for recovery. E_{Na}, E_{K} are the Na^+, K^+ reversal potentials, and g_{Na}, g_{K} are the respective ion-channel conductances. The first equation expresses the total membrane current CdV/dt as the sum of Na^+ and K^+ ionic currents in the form (channel conductance) $\times$ (driving voltage), to which is added a dc stimulus current I_{dc} plus a white-noise current $\sigma_I\xi_1(t)$ of rms amplitude σ_I. The second equation describes the noisy evolution of the recovery variable R to its steady-state value $G(V)$ perturbed by a small dimensionless white-noise disturbance $\sigma_R\xi_2(t)$. By changing the form of $G(V)$ from a linear polynomial to a quadratic, the Wilson model is capable of simulating spike generation in *either* a squid axon (resonator) *or* in a human cortical neuron (integrator).

The parameter values and polynomial coefficients for Wilson's squid axon and human neuron models are listed in Table I.

By assumption, the $\xi_{1,2}(t)$ white-noise sources in Eqs. (1) are a pair of independent, Gaussian-distributed random time series of zero mean, infinite variance, with delta-function correlation in time,

$$\langle\xi(t)\rangle = 0, \quad \langle\xi_j(t)\xi_k(t')\rangle = \delta_{j,k}\delta(t-t'). \tag{2}$$

In the stochastic numerical simulations that follow, an approximation for each infinite-variance time series is constructed by drawing samples from a zero-mean, *unit*-variance Gaussian random number generator, $\mathcal{R}(0,1)$, scaled by the square-root of the inverse of the time step, Δt,

$$\xi(t) = \frac{\mathcal{R}_n(0,1)}{\sqrt{\Delta t}}, \tag{3}$$

where $t=n\Delta t$ is discrete time for sample n. By design, these scaled random numbers have variance $1/\Delta t$, rendering the required delta-function correlation in the continuous limit $\Delta t \to 0$.

Although the inclusion of a *single* noise source in the Wilson model would have been sufficient to explore its stochastic response, we have elected to include *two* independent noises, ξ_1 and ξ_2, to better represent the biological reality that there are multiple sources of uncertainty in a living cell, and

TABLE I. Definitions and constants for the Wilson [24] model for squid axon (second column) and human cortical neuron (third column) with additive noise. Note that both here and in Eq. (1) the reversal potentials (E_{Na},E_K) and the membrane voltage V are expressed in decivolts, thus they must be scaled by 100 to retrieve their millivolt values (e.g., $E_{Na}=0.48=+48$ mV). Similarly, each current must be scaled by 100 to retrieve its physical value in $\mu A/cm^2$. I_{dc}^{crit} is the threshold input current for spike generation.

Symbol	Squid	Human	Unit
C	0.8	1.0	$\mu F/cm^2$
τ_R	1.9	5.6	ms
E_{Na}, E_K	0.55, −0.92	0.48, −0.95	10^2 mV
$g_{Na}(V)$	$g_1(V)$[a]	$g_2(V)$[b]	mS/cm^2
g_K	26.0	26.0	mS/cm^2
$G(V)$	$G_1(V)$[c]	$G_2(V)$[d]	
σ_I	0.001	0.01	10^2 $\mu A\ cm^{-2}(ms)^{1/2}$
σ_R	0.001	0.01	$10^2(ms)^{1/2}$
I_{dc}^{crit}	~0.0777327	~0.214752	10^2 $\mu A/cm^2$

[a] $g_1(V)=32.63V^2+47.71V+17.81$.
[b] $g_2(V)=33.80V^2+47.58V+17.81$.
[c] $G_1(V)=1.35V+1.03$.
[d] $G_2(V)=3.30V^2+3.798V+1.267$.

that the uncertainties in currents entering the cell that accumulate to trigger a voltage spike are likely to be independent of the uncertainties associated with the recovery dynamics following a spike. The choice of white noise (rather than correlated noise) is a mathematical convenience that allows us to compute fluctuation statistics that are exact in the small-noise limit, but we note that exaggerated responsiveness to small perturbation is a robust near-threshold property that is largely independent of the spectral character of the perturbation (see Sec. III of [30] for further discussion).

A. Approach to threshold

The fact that Eqs. (1) are capable of generating realistic type-I and -II spike trains is already well-established (e.g., see Chap. 9 of Wilson's book [24]), so this aspect will not capture much attention here. Instead, we will be concentrating on the "quiet" time during which the subthreshold neuron appears to be "doing nothing," and we ask, What can we learn about the state of the neuron by attending to its stochastic microscale voltage fluctuations? We will find that the "jitteriness" or responsiveness of an excitable membrane depends on the amplitude of the injected dc current, or, more precisely, on how close I_{dc} is to a critical threshold value, I_{dc}^{crit}.

Figure 1 shows a series of numerical simulations of the stochastic Wilson equations for both (a) squid axon, and (b) human cortical neuron, at five values of subthreshold stimulus current I_{dc}. For each membrane type, the white-noise sequences generated for $\sigma_I\xi_1(t)$ and for $\sigma_R\xi_2(t)$ at the lowest stimulus current were reused in each of the higher stimulus trials. As the threshold current is approached from below, the noise-driven squid axon in Fig. 1(a) shows an increasing tendency to "ring" at a characteristic frequency, with the reverberations becoming larger and less damped at larger dc stimulus values. These subthreshold oscillations break over into repetitive full-scale spiking when the random fluctuations cause the membrane voltage to cross threshold—see top trace of Fig. 1(a).

The Fig. 1(b) time series for the human neuron model show a very different temporal structure from that obtained for the squid axon model. Rather than inducing ringing patterns, larger stimulus currents cause the membrane voltage trace to become "noisier," with high-frequency fluctuations riding an ever-slowing low-frequency envelope. When eventually the fluctuations carry the membrane voltage across a critical value, the neuron generates a single isolated action potential, rather than the cluster of regular spikes seen in the squid case. Scanning the top trace of Fig. 1(b), the evolution of the cortical membrane voltage—from noisy quiescence to spike generation—reminds us of Carmichael's [36] description of a state change (in quantum optics) in which the process

> "…amplifies the initial fluctuations up to the macroscopic scale, making it impossible to disentangle a mean motion from the fluctuations."

Prior to spike onset, is the slowly varying trend a fluctuation about the mean, or the mean motion itself? Carmichael tells us that near a change of state (the birth of an action potential), the fluctuation and the mean motion are one and the same. This insight also holds for the resonator membrane traces of Fig. 1(a).

These graphs confirm that the stochastic versions of the Wilson model retain the respective resonator (i.e., repetitive regular firing) and integrator (firing at arbitrarily low frequency) behaviors expected of type-II and -I membranes. We will now demonstrate that enhanced near-threshold resonator (or integrator) responsiveness is not a uniquely stochastic property: tuned responsiveness is also an inherent feature of the *noise-free* Wilson equations. In fact, we will find that understanding the *eigenvalue structure* of the noiseless Wilson equations is key to understanding the membrane's current-dependent sensitivity to noisy stimulation.

B. Staircase impulse response

To demonstrate the squid model's inherent responsiveness to abrupt changes in subthreshold stimulus current, we set the noise amplitudes σ_I and σ_R to zero in Eqs. (1), then drive the Wilson type-II model with a staircase-shaped injected current. The initial stimulus current $I_{dc}(t=0)$ is -4 $\mu A/cm^2$ (i.e., a conventional current of magnitude 4 $\mu A/cm^2$ directed *outwards* from the nerve cell); at $t=30$ ms the current is reset to -1.67 $\mu A/cm^2$, held at this level for 60 ms, then stepped consecutively to +0.66, +2.99, +5.32, and +7.65 $\mu A/cm^2$ at successive 60-ms intervals. There are a total of five equal increments in stimulus current during the 300-ms duration of the numerical experiment. The results appear in Fig. 2.

The time series in Fig. 2(a) shows the $V(t)$ membrane voltage response to each of the five current steps, and (b) shows the corresponding phase plot obtained by plotting $V(t)$ against $R(t)$, the time series for the recovery variable. It is

very clear from these graphs that (i) the type-II membrane responds to an impulsive current change with a characteristic ringing pattern; (ii) the ringing becomes more persistent as the stimulus current approaches the threshold for spiking; and (iii) the amplitude of the membrane response increases strongly as I_{dc} approaches threshold. Note that after the fifth current step at $t=270$ ms, I_{dc} is almost at the threshold value of $I_{dc}^{crit} \approx 7.77327\ \mu A/cm^2$, and the oscillation decays extremely slowly (time constant $\sim$250ms), the heavy trace appearing in (b) actually being an exceptionally gradual inwards spiral. For $I_{dc} \gtrsim I_{dc}^{crit}$, the phase plot would spiral outwards (not shown here), eventually evolving into a large-scale nonlinear limit cycle that defines the action potential. If $I_{dc}=I_{dc}^{crit}$, the membrane oscillation would be delicately balanced between growth and decay, and, in principle, the oscillation would persist forever. In this limit, the squid membrane has become an *ideal resonator*.

We now perform a closely similar staircase impulse-response experiment on the noiseless Wilson type-I neuron. See Fig. 3. The cortical neuron staircase response shows none of the overshoot-ringing structure that dominates the squid response. Instead, we see in Fig. 3(a) that the type-I membrane responds to a step change in current on two distinct time scales. The initial response is very fast and rapidly decaying, appearing as the near-vertical edge immediately following the step events at $t=30$, 90, 150, 210, and 270 ms. This is followed by a much slower exponential decay, with a time constant that becomes more prolonged for current steps that take the membrane closer to spiking threshold. This dual time-scale structure is made more visible in Fig. 3(b) where we have subtracted the staircase of equilibrium voltages from the $V(t)$ time series. Also evident in Fig. 3(b) is the increase in membrane sensitivity to step perturbations as the injected current approaches threshold. In Fig. 3(c) we replot the logarithm of the ΔV residuals against a lag-time axis that is reset to zero with each step. The four $1/e$ slow-decay times, extracted from the inverse-slopes, are (1) 9.7; (2) 10.6; (3) 12.2; and (4) 17.2 ms.

C. Eigenvalue analysis

Figures 2 and 3 show that, as the dc stimulus current I_{dc} is increased towards spiking threshold, the two classes of excitable membrane exhibit *stronger* and *more persistent* step-evoked impulse responses, with divergence in both characteristics (amplitude *and* duration) at threshold. This inverse sensitivity to distance from threshold can be explained in terms of the I_{dc}-dependent eigenvalue structure of the linearized Wilson equations.

The eigenvalue analysis proceeds as follows. We zero the noise amplitudes σ_I, σ_R, and write Eqs. (1) in their noise-free form,

$$F_1(V,R) = \frac{1}{C}[-g_{Na}(V)(V-E_{Na}) - g_K R(V-E_K) + I_{dc}], \tag{4a}$$

$$F_2(V,R) = \frac{1}{\tau_R}[-R + G(V)], \tag{4b}$$

where $F_1 \equiv dV/dt$ and $F_2 \equiv dR/dt$. We fix a value for the I_{dc} stimulus current, set to zero the time-derivatives dV/dt, dR/dt, and solve numerically the resulting (polynomial) equations (4), giving the steady-state coordinate (V^o,R^o) for membrane voltage and recovery variable. We then compute the 2×2 Jacobian matrix of partial derivatives, **J**, evaluated at this (V^o,R^o) equilibrium point,

$$\mathbf{J} = \begin{bmatrix} \frac{\partial F_1}{\partial V} & \frac{\partial F_1}{\partial R} \\ \frac{\partial F_2}{\partial V} & \frac{\partial F_2}{\partial R} \end{bmatrix}_{|(V^o,R^o)} . \tag{5}$$

The eigenvalues of **J** predict the exponential time course (growth or decay) for small fluctuations about the (V^o,R^o) equilibrium point, and hence its stability: if both eigenvalues are real and negative (or are complex with negative real parts), then fluctuations will decay and the equilibrium point is *stable*; if either eigenvalue is positive (or, for complex eigenvalue pairs, if the pair has a positive real part), then the equilibrium is *unstable*.

Note that these eigenvalues are only valid for a given equilibrium point. Because the location of the steady-state coordinate is determined by the magnitude and direction of the injected dc current, any alteration in I_{dc} mandates a recalculation of the steady-state, its Jacobian, and the eigenvalues it owns.

Figures 4 and 5, respectively, show the distribution of steady states and eigenvalues for the Wilson models for the squid axon (resonator) and human neuron (integrator) excitable membranes. For the squid, the eigenvalues λ_1 and λ_2 form a complex-conjugate pair, $\lambda_{1,2}=-\alpha \pm i\omega_o$, with a sign change in α, the damping, when the stimulus current crosses the critical value $I_{dc}^{crit} \approx 7.7733\ \mu A/cm^2$. For $I_{dc}<I_{dc}^{crit}$, the equilibrium point is stable, and perturbations are predicted to decay with a $1/e$ time constant $T_{slow}=1/\alpha$, showing damped oscillations, of frequency f_o, determined by the imaginary part of the eigenvalues: $f_0=\omega_o/2\pi$; these predictions are consistent with the ringing behaviors recorded in the staircase impulse responses of Fig. 2. For $I_{dc}>I_{dc}^{crit}$, the equilibrium point is unstable, so any perturbation will grow exponentially, evolving into a full-scale action-potential spike. At $I_{dc}=I_{dc}^{crit}$, damping vanishes, so $T_{slow}\to\infty$; thus the linearized theory predicts the precarious possibility of a state delicately poised between either infinitely slowed quiescence or progression to firing.

Figure 5 shows the corresponding distribution of steady states and eigenvalues for the Wilson model for the mammalian cortical neuron. Unlike the squid axon, the cortical neuron possesses up to *three* steady states for a given value of stimulus current; at each of these three (V^o,R^o) fixed points, we find that both eigenvalues are real. The Fig. 5(b) eigenvalue map shows that the dominant eigenvalue changes sign at a critical current $I_{dc}^{crit} \approx 21.475\ \mu A/cm^2$; this occurs at the lower turning point in the S-bend of steady states in panel (a). Stimulus currents higher than this critical value will destabilize the membrane, leading to the firing of action potentials. For $I_{dc}<I_{dc}^{crit}$, only the lower branch of equilibrium points is stable, and, along this branch, perturbations are predicted to decay to rest over two quite distinct time-scales, $T_{slow}=-1/\lambda_1$ and $T_{fast}=-1/\lambda_2$. This is consistent with the

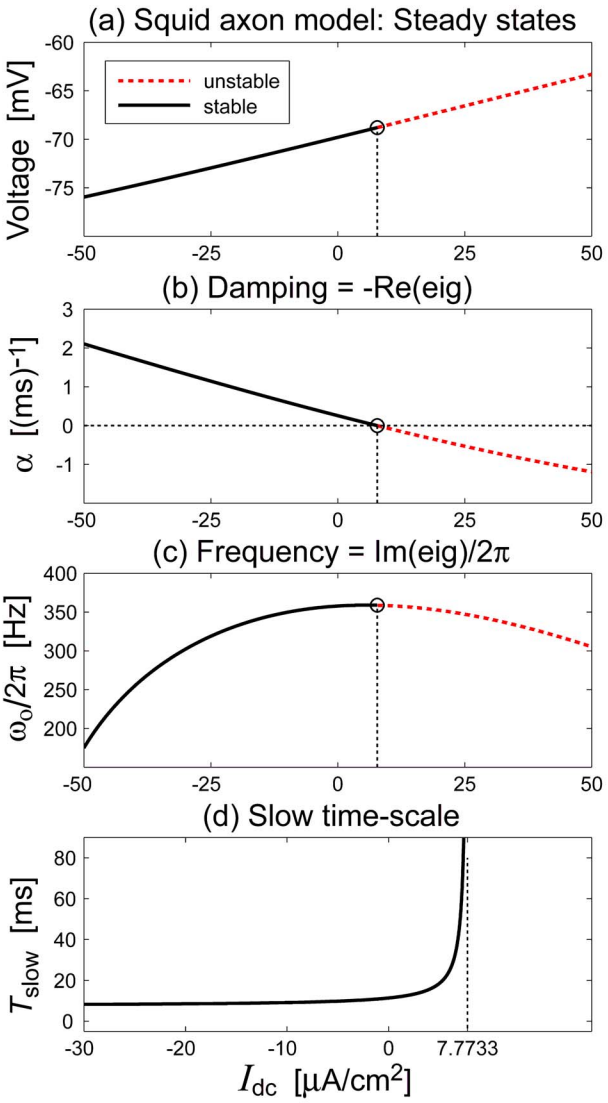

FIG. 4. (Color online) Steady states and eigenvalues for the Wilson type-II squid membrane in the vicinity of the threshold for firing. (a) Steady-state membrane voltage as a function of dc stimulus current. When stimulus current exceeds threshold, $I_{dc}^{crit} \approx 7.77327\ \mu A/cm^2$, the steady state becomes unstable with respect to small perturbations, and full-scale action potential spikes emerge [see top trace of Fig. 1(a)]. (b) and (c) Near threshold, the two eigenvalues for the linearized Wilson squid axon form a complex-conjugate pair, $\lambda_{1,2}=-\alpha \pm i\omega_o$, where α is the damping rate constant, and $\omega/2\pi$ is the oscillatory frequency. For $I_{dc}<I_{dc}^{crit}$, the damping is positive, and the squid impulse response shows damped oscillations; for $I_{dc}>I_{dc}^{crit}$, the damping is negative, the oscillations explode exponentially, and evolve into large-scale limit cycles (action potentials). When $I_{dc}=I_{dc}^{crit}$, the damping is precisely zero, and the small-scale subthreshold ringing patterns persist forever. (d) The inverse of the decay rate defines the time scale over which perturbations about steady state die away: $T_{slow}=1/\alpha$ (for $\alpha>0$). At the critical point, $\alpha \to 0$ and $T_{slow} \to \infty$. This divergence curve determines the growth envelope for the voltage fluctuations in a white-noise-driven squid axon approaching threshold [see Fig. 6(a)].

two-exponential decays seen in the Fig. 3 staircase response. As is the case for the squid membrane, the T_{slow} slow time scale diverges to infinity as $I_{dc} \to I_{dc}^{crit}$ from below. We will see, in the stochastic analysis which follows, that this divergence in the slow time scale controls the growth in fluctuation *amplitude* when an excitable membrane is disturbed by white noise.

III. SUBTHRESHOLD STOCHASTIC THEORY

We assume that the membrane is resting at the quiescent subthreshold equilibrium point (V^o, R^o) defined by a preset level of injected current I_{dc} entering the soma. Following Eqs. (1), we impose a pair of independent low-intensity white noises as additive perturbations: $\sigma_I \xi_1(t)$ adds noise to the injected current, and $\sigma_R \xi_2(t)$ imposes a random jitter to the Na^+/K^+ recovery. Provided that the noise intensities are sufficiently weak, the noise-evoked subthreshold fluctuations in recovery variable R and membrane voltage V will be rather small, so a linear analysis of the Wilson equations should give a valid description here. By *fluctuation*, we mean the instantaneous deviation away from the (V^o, R^o) equilibrium:

$$v(t) = V(t) - V^o, \tag{6a}$$

$$r(t) = R(t) - R^o. \tag{6b}$$

It is important to emphasize that if the I_{dc} stimulus current is altered, then the (V^o, R^o) equilibrium point for the fluctuations must be recomputed, since this reference coordinate, being determined by intersection of the isoclines of Eqs. (1), varies with I_{dc}.

We linearize Eqs.(1) about a (subthreshold) steady state, giving the matrix equation,

$$\frac{d}{dt}\begin{bmatrix} v \\ r \end{bmatrix} = -\mathbf{A}\begin{bmatrix} v \\ r \end{bmatrix} + \sqrt{\mathbf{D}}\begin{bmatrix} \xi_1(t) \\ \xi_2(t) \end{bmatrix}, \tag{7}$$

where $\mathbf{A}$, the 2×2 *drift* matrix, is equal to the negative of the Jacobian matrix, $\mathbf{J}$, evaluated at the nominated steady state, i.e., $\mathbf{J}=-\mathbf{A}$. Here, $\mathbf{D}$ is the constant *diffusion* matrix,

$$\mathbf{D} = \begin{bmatrix} \sigma_I^2/C^2 & 0 \\ 0 & \sigma_R^2/\tau_R^2 \end{bmatrix}. \tag{8}$$

A. Covariance matrix

Equations (7) define a two-dimensional Ornstein-Uhlenbeck (Brownian motion) process. Following Gardiner [20] we can immediately write down exact expressions for the variances and covariances of the fluctuation time series for membrane voltage v and recovery r. Defining the covariance matrix as

$$\mathbf{\Sigma} \equiv \begin{bmatrix} \mathrm{var}\{v\} & \mathrm{cov}\{v,r\} \\ \mathrm{cov}\{r,v\} & \mathrm{var}\{r\} \end{bmatrix}, \tag{9}$$

its theoretical value can be computed exactly from

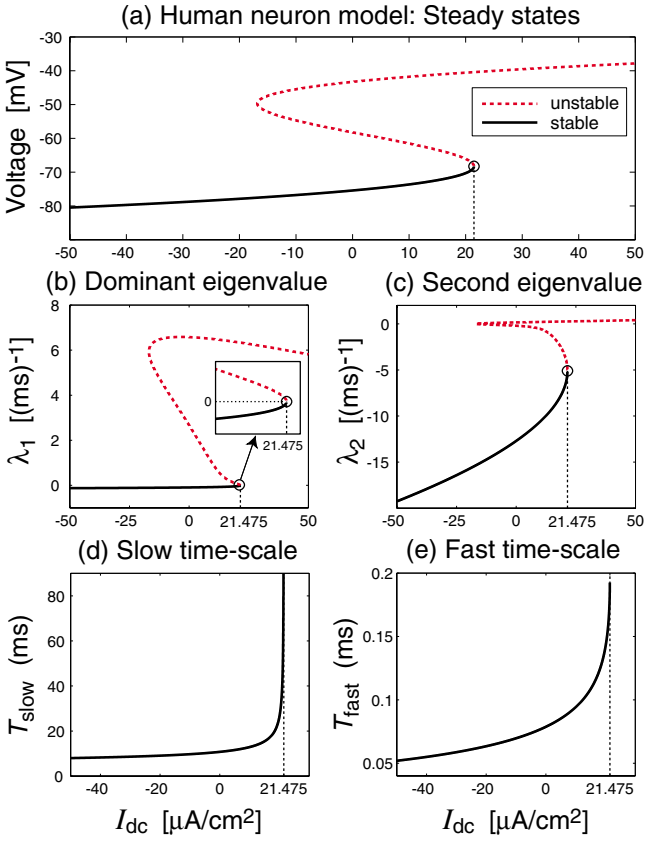

FIG. 5. (Color online) Steady states and eigenvalues for the Wilson type-I cortical neuron in the vicinity of the firing threshold. (a) S-bend distribution of steady-state membrane voltages as a function of dc stimulus current. Only the bottom branch (solid black) is stable with respect to small perturbations; the middle and top branches (drawn with a thick dashed red line) are unstable. For a neuron started on the bottom branch, an increase in I_{dc} beyond the threshold point $I_{dc}^{crit} \approx 21.4752\ \mu A/cm^2$ (marked with a "o" symbol) destabilizes the membrane, and a full-scale spike is generated [see top trace of Fig. 1(b)]. (b) and (c) Below threshold, both eigenvalues for the linearized Wilson cortical neuron are real and negative, with the dominant eigenvalue, λ_1, approaching zero from below as $I_{dc} \to I_{dc}^{crit}$. For the midbranch steady states, $\lambda_1 > 0$ and $\lambda_2 < 0$, defining a saddle instability. Along the top branch, both eigenvalues are positive. (d) and (e) Below threshold, the dominant and second eigenvalues, respectively, determine the slow and fast time scales for relaxation back to steady state: $T_{slow} = -1/\lambda_1$, $T_{fast} = -1/\lambda_2$, with $T_{slow} \to \infty$ as $\lambda_1 \to 0$. The divergence of the slow time scale is responsible for the divergent growth in dc fluctuation power as the white-noise-driven integrator neuron approaches spiking threshold (see Fig. 8).

$$\mathbf{\Sigma} = \frac{\det(\mathbf{A})\mathbf{D} + [\mathbf{A} - \mathrm{tr}(\mathbf{A})\mathbf{I}]\mathbf{D}[\mathbf{A} - \mathrm{tr}(\mathbf{A})\mathbf{I}]^{\mathrm{T}}}{2\,\mathrm{tr}(\mathbf{A})\det(\mathbf{A})}, \qquad (10)$$

where $\mathbf{I}$ is the 2×2 identity matrix; $\det(\cdot)$ and $\mathrm{tr}(\cdot)$ are the determinant and trace operators. Here we will focus on $\mathrm{var}\{v\}$, the variance of the voltage fluctuations. Expanding the matrix multiplications of Eq. (10) and extracting the Σ_{11} entry gives

$$\Sigma_{11} \equiv \mathrm{var}\{v\} = \frac{\det(\mathbf{A})D_{11} + A_{22}^2 D_{11} + A_{12}^2 D_{22}}{2\,\mathrm{tr}(\mathbf{A})\det(\mathbf{A})}. \qquad (11)$$

From standard matrix theory [37], we can express the trace and determinant expressions, respectively, as the sum and product of $\lambda_{1,2}$, the eigenvalues of the Jacobian matrix $\mathbf{J} = -\mathbf{A}$,

$$\mathrm{tr}(\mathbf{A}) = -\mathrm{tr}(\mathbf{J}) = -(\lambda_1 + \lambda_2),$$

$$\det(\mathbf{A}) = \det(\mathbf{J}) = \lambda_1 \lambda_2,$$

giving a final form for the fluctuation variance that makes clear its crucial dependence on the eigenvalue structure of the excitable membrane's equilibrium Jacobian,

$$\mathrm{var}\{v\} = \frac{\lambda_1\lambda_2 D_{11} + A_{22}^2 D_{11} + A_{12}^2 D_{22}}{-2(\lambda_1 + \lambda_2)\lambda_1\lambda_2}. \qquad (12)$$

We will see that for both resonator and integrator excitable membrane types, the approach to threshold will be associated with a divergent growth in fluctuation power, but with scaling laws and spectral distributions that are quite distinct.

1. Resonator approach to threshold

The Jacobian for the subthreshold resonator (type-II) membrane has a pair of complex-conjugate eigenvalues of the form $\lambda_{1,2} = -\alpha \pm i\omega_o$, with damping $\alpha > 0$. Equation (12) gives

$$\mathrm{var}\{v\}^{\mathrm{Res}} = \frac{(\alpha^2 + \omega_o^2)D_{11} + A_{22}^2 D_{11} + A_{12}^2 D_{22}}{4\alpha(\alpha^2 + \omega_o^2)}, \qquad (13)$$

which, in the limit of small damping, reduces to

$$\mathrm{var}\{v\}^{\mathrm{Res}} \approx \frac{1}{\alpha}\frac{\omega_o^2 D_{11} + A_{22}^2 D_{11} + A_{12}^2 D_{22}}{4\omega_o^2}. \qquad (14)$$

From Fig. 4(b), the damping goes linearly to zero as the dc stimulus current approaches its critical value I_{dc}^{crit}, thus our Ornstein-Uhlenbeck theory predicts that the variance of the resonator voltage fluctuations will *diverge to infinity* at the threshold for spiking:

$$I_{dc} \to I_{dc}^{crit} \Rightarrow \alpha \to 0 \Rightarrow \mathrm{var}\{v\}^{\mathrm{Res}} \to \infty.$$

If we define a nondimensional distance to threshold as $\epsilon = (I_{dc}^{crit} - I_{dc})/I_{dc}^{crit}$, then we can deduce that the scaling law for this divergence will be

$$\mathrm{var}\{v\}^{\mathrm{Res}} \sim \frac{1}{\epsilon}. \qquad (15)$$

This follows because $\mathrm{var}\{v\}^{\mathrm{Res}} \sim 1/\alpha$, and, near threshold, $\alpha \sim I_{dc}$.

2. Integrator approach to threshold

The Jacobian for the subthreshold integrator (type-I) membrane has a pair of real eigenvalues, both negative: $\lambda_2 < \lambda_1 < 0$. On approach to spiking threshold, the dominant

eigenvalue tends to zero from below: $\lambda_1 \to 0^-$ [see Fig. 5(b)]. In the limit of small λ_1, Eq. (12) gives

$$\mathrm{var}\{v\}^{\mathrm{Int}} \approx \frac{1}{-\lambda_1}\frac{A_{22}^2 D_{11} + A_{12}^2 D_{22}}{2\lambda_2^2}, \quad \lambda_1 < 0. \tag{16}$$

Thus, like the squid resonator, linearized theory predicts the cortical integrator membrane will become infinitely responsive to white-noise perturbations, with the variance of the voltage fluctuations diverging to infinity at the threshold for spiking:

$$I_{\mathrm{dc}} \to I_{\mathrm{dc}}^{\mathrm{crit}} \Rightarrow \lambda_1 \to 0^- \Rightarrow \mathrm{var}\{v\}^{\mathrm{Int}} \to \infty.$$

However, unlike the squid axon, the fluctuation divergence for the cortical neuron will follow a *fractional* power-scaling law:

$$\mathrm{var}\{v\}^{\mathrm{Int}} \sim \frac{1}{\sqrt{\epsilon}}. \tag{17}$$

This claim is justified as follows. For the type-I neuron, the threshold for spiking occurs when two sets of steady states—one set from the unstable saddle on the midbranch, the other set from the line of stable nodes on the bottom branch—come together at the lower turning point of the S-bend of steady states. This point, marked "o" in Fig. 5(a), is the saddle-node annihilation point (or, viewed in the direction of decreasing current, is the saddle-node *bifurcation* point). Because this bifurcation point straddles the two solution-branches, the approach to threshold will show a locally parabolic [40]—rather than linear—relationship between steady-state voltage and ϵ, the displacement of I_{dc} from its threshold value, $\epsilon = (I_{\mathrm{dc}}^{\mathrm{crit}} - I_{\mathrm{dc}})/I_{\mathrm{dc}}^{\mathrm{crit}}$. The zoomed inset in Fig. 5(b) also exhibits a locally parabolic relationship between the dominant eigenvalue λ_1 and displacement from threshold: $\lambda_1 \sim -\sqrt{\epsilon}$. This establishes the scaling law (17) for integrator-neuron divergence.

We note that this square-root scaling law is a very general feature of systems that are close to a saddle-node bifurcation—see p. 99 of Strogatz [18].

3. White-noise susceptibility

Referring to Eq. (12), we see that the fluctuation power *output* of a subthreshold membrane depends explicitly on the intensities, D_{11} and D_{22}, of the $\xi_1(t)$ and $\xi_2(t)$ white-noise *inputs*. In order to quantify the sensitivity of the membrane to white-noise stimulation, we divide through by D_{11} to give a form of transfer ratio that we define as the *white-noise susceptibility*, χ:

$$\chi \equiv \frac{\Sigma_{11}}{D_{11}} = \frac{\lambda_1\lambda_2 + A_{22}^2 + kA_{12}^2}{-2(\lambda_1+\lambda_2)\lambda_1\lambda_2}, \tag{18}$$

where we have assumed $D_{22}/D_{11} = k$, a constant; that is, the intensities for the $\xi_1(t)$ and $\xi_2(t)$ sources are in fixed ratio. This assumption is true for our stochastic implementation of the Wilson type-I and -II membranes, for which, from Eq. (8), we obtain $k = (\sigma_R C/\sigma_I \tau_R)^2$.

From Eq. (18) we see that the divergence properties are unchanged by the D_{11} normalization, consequently the scaling laws for resonator and integrator susceptibility match those previously stated in Eqs. (15)–(17) for resonator and integrator variance. See Table II for a summary.

TABLE II. Summary of dynamic properties and scaling laws for the white-noise-driven subthreshold squid membrane and human neuron models. Here, ϵ is the dimensionless distance below threshold: $\epsilon = (I_{\mathrm{dc}}^{\mathrm{crit}} - I_{\mathrm{dc}})/I_{\mathrm{dc}}^{\mathrm{crit}}$. The susceptibility, χ, quantifies the fluctuation-power responsiveness of the membrane to white-noise stimulation: $\chi = \Sigma_{11}/D_{11}$.

Property	Squid	Human
Equalities		
Damping, α	$-\mathrm{Re}(\lambda_{1,2})$	$-\lambda_1$
Resonant frequency, ω_o	$-\mathrm{Im}(\lvert\lambda_{1,2}\rvert)$	0
Scaling laws		
Correlation time, T_{slow}	$\sim 1/\epsilon$	$\sim 1/\sqrt{\epsilon}$
Susceptibility, χ	$\sim 1/\epsilon$	$\sim 1/\sqrt{\epsilon}$

B. Time-correlation matrix

The 2×2 steady-state time-correlation matrix for the time series of v and r fluctuations is defined,

$$\mathbf{C}(\tau) \equiv \begin{bmatrix} \mathrm{cov}\{v(0),v(\tau)\} & \mathrm{cov}\{v(0),r(\tau)\} \\ \mathrm{cov}\{r(0),v(\tau)\} & \mathrm{cov}\{r(0),r(\tau)\} \end{bmatrix}, \tag{19}$$

where τ is the lag-time. For an Ornstein-Uhlenbeck process, Gardiner [20] gives an exact expression for $\mathbf{C}(\tau)$ as the product of the matrix exponential $\exp(-\mathbf{A}\tau)$ with the covariance matrix $\mathbf{\Sigma}$:

$$\mathbf{C}(\tau) = e^{-\mathbf{A}\tau}\mathbf{\Sigma}, \quad \tau \geqslant 0 \tag{20}$$

with symmetry property $\mathbf{C}(-\tau) = [\mathbf{C}(\tau)]^{\mathrm{T}}$. While Eq. (20) is computationally convenient (and, in fact, was used to compute the theoretical autocorrelation functions displayed in Figs. 7 and 9), an alternate form that better lends itself to insight can be derived by expressing the matrix exponential in terms of the eigenvalues $\lambda_{1,2}$ and eigenvectors $\vec{r}_{1,2}$ of $\mathbf{J} = -\mathbf{A}$, the Jacobian matrix evaluated at equilibrium. Then Eq. (20) becomes

$$\mathbf{C}(\tau) = [\vec{r}_1 \quad \vec{r}_2]\begin{bmatrix} e^{\lambda_1\tau} & 0 \\ 0 & e^{\lambda_2\tau} \end{bmatrix}[\vec{r}_1 \quad \vec{r}_2]^{-1}\mathbf{\Sigma}. \tag{21}$$

Expanding, then selecting the terms for the $C_{11}(\tau)$ element to extract the autocorrelation function for the $v(t)$ fluctuations in membrane voltage, we obtain,

$$C_{11}(\tau) = c_1 e^{\lambda_1\tau} + c_2 e^{\lambda_2\tau} \quad \text{(integrator neuron)} \tag{22}$$

indicating that the autocorrelation function for the voltage fluctuations is a linear combination of *two exponential-decay processes* whose rate constants are the eigenvalues of the Jacobian matrix. (The relative weighting of the exponentials, given by c_1 and c_2, depends on the Σ_{11} and Σ_{21} entries of the $\mathbf{\Sigma}$ covariance matrix, and on the components of the $\vec{r}_1$ and $\vec{r}_2$ eigenvectors—but we do not state their explicit form here.)

Equation (22) is directly applicable to the integrator neuron whose subthreshold Jacobian owns a pair of real eigen-

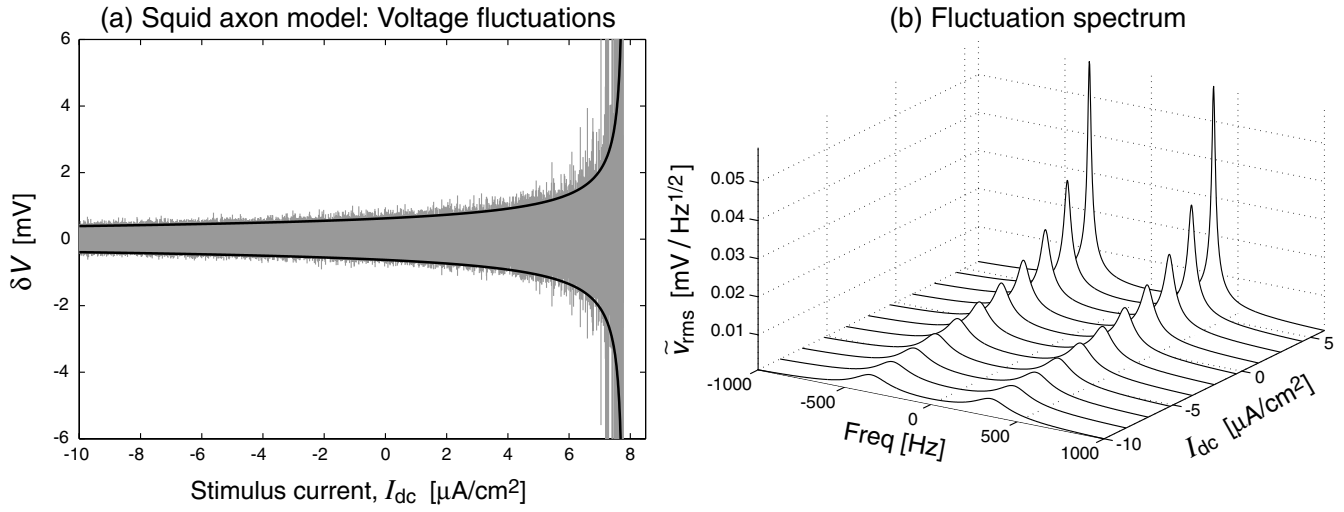

FIG. 6. Model squid-membrane subthreshold response to white-noise perturbation as a function of I_{dc} stimulus current. (a) Solid black curves show predicted $\pm 3\sigma$ limits for voltage excursions away from equilibrium; each vertical gray trace shows actual maximum excursions recorded in a 200-ms stochastic simulation run of the Wilson Eqs. (1) at each of 2000 settings for stimulus current ranging from -10.0 to $+7.77$ μA/cm^2. Fluctuation intensity grows strongly on approach to the critical current required for spike generation. (b) Theoretical spectral response to white-noise driving for the squid axon model. The double-sided spectrum develops a pronounced and increasingly narrow resonance at $\sim \pm 360$ Hz as the critical current is approached from below.

values, both negative: $\lambda_2 < \lambda_1 < 0$. On approach to threshold, the dominant eigenvalue goes to zero, and the leading exponential term $\exp(\lambda_1 \tau)$ will exhibit critical slowing, becoming infinitely persistent at threshold when λ_1 is precisely zero. Since this linear analysis assumes small fluctuations, Eq. (22) tells us the limits of its validity: when the membrane crosses threshold and λ_1 goes positive, the voltage autocorrelations will explode exponentially, violating the smallness assumption. At this point the nonlinear dynamics take over, and a spike is born. Since $\lambda_1 > 0$ defines the region of spike generation, and $\lambda_1 < 0$ defines the region of stable stochastics, the case $\lambda_1 = 0$ is very special, since not only does it mark the extremum of critically slowed microscale linear stochastics, but it also identifies the seed-point for the genesis of gross-scale nonlinear dynamics.

For the squid resonator, the eigenvalues associated with its subthreshold Jacobian are a complex-conjugate pair $\lambda_{1,2} = -\alpha \pm i\omega_o$, with $\alpha > 0$. After a little algebraic manipulation, Eq. (22) can be reworked into the form

$$C_{11}(\tau) = c_1 e^{-\alpha\tau} \cos(\omega_o \tau) \quad \text{(squid membrane)}. \tag{23}$$

Thus the autocorrelation function for the squid voltage fluctuations corresponds to the impulse response of a damped oscillator of frequency ω_o and damping α. As the squid axon approaches threshold, $\alpha \to 0$, and the ringing becomes more and more long-lived, becoming infinitely persistent at threshold when $\alpha = 0$. Above threshold, α changes sign and the exponential term explodes, signaling the demise of the linear theory as the membrane changes phase from stochastic quiescence to active spiking.

C. Spectrum matrix

The Fourier transform of $\mathbf{C}(\tau)$ gives the 2×2 spectrum matrix [20],

$$\mathbf{S}(\omega) = \frac{1}{2\pi} \int_{-\infty}^{\infty} e^{-i\omega\tau} \mathbf{C}(\tau) d\tau = \frac{1}{2\pi} (\mathbf{A} + i\omega \mathbf{I})^{-1} \mathbf{D} (\mathbf{A}^{\mathrm{T}} - i\omega \mathbf{I})^{-1}. \tag{24}$$

Here we will focus on the $S_{11}(\omega)$ component of the spectral matrix, since this element gives the power spectral density of the voltage fluctuations. Expanding Eq. (24) and extracting the S_{11} terms gives

$$S_{11}(\omega) = \frac{1}{2\pi} \frac{A_{22}^2 D_{11} + A_{12}^2 D_{22} + D_{11}\omega^2}{(\lambda_1 \lambda_2 - \omega^2)^2 + (\lambda_1 + \lambda_2)^2 \omega^2}. \tag{25}$$

1. Cortical-neuron spectrum

For the subthreshold cortical neuron, the Jacobian eigenvalues are real and negative, $\lambda_2 < \lambda_1 < 0$. On approach to spiking threshold, the dominant eigenvalue tends to zero, and, at threshold, Eq. (25) predicts the limiting spectrum,

$$\lim_{\lambda_1 \to 0} S_{11}(\omega) = \frac{1}{2\pi} \frac{A_{22}^2 D_{11} + A_{12}^2 D_{22} + D_{11}\omega^2}{\omega^4 + \lambda_2^2 \omega^2} \quad \text{(integrator neuron)} \tag{26}$$

which is divergent at $\omega = 0$. This pole at zero frequency means that at threshold, the integrator neuron becomes *resonant at dc*. This is consistent with the time-domain analysis which showed that the fluctuation autocorrelation function will be dominated by a single exponential decay of infinite persistence, implying that its Fourier transform will be a delta-function at zero frequency.

2. Squid-axon spectrum

The subthreshold squid axon has a pair of complex conjugate eigenvalues, $\lambda_{1,2} = -\alpha \pm i\omega_o$, with $\alpha > 0$. Substituting in Eq. (25) gives

$$S_{11}(\omega) = \frac{1}{2\pi} \frac{A_{22}^2 D_{11} + A_{12}^2 D_{22} + D_{11}\omega^2}{(\alpha^2 + \omega_o^2 - \omega^2)^2 + 4\alpha^2\omega^2}. \quad (27)$$

At spiking threshold the damping goes to zero, so the limiting fluctuation spectrum will be

$$\lim_{\alpha \to 0} S_{11}(\omega) = \frac{1}{2\pi} \frac{A_{22}^2 D_{11} + A_{12}^2 D_{22} + D_{11}\omega^2}{(\omega_o^2 - \omega^2)^2} \quad \text{(squid axon)} \quad (28)$$

implying infinite power at $\omega = \omega_o$.

IV. STOCHASTIC SIMULATION RESULTS

To test the predictions of the subthreshold stochastic theory, we ran a series of numerical simulations of the noise-perturbed Wilson equations (1), both for the squid-axon resonator (see second column of Table I) and for the cortical-neuron integrator (third column of Table I).

A. Squid-axon stochastic response

Figure 6(a) summarizes the outcome of 2000 separate 200-ms stochastic realizations of the squid-axon Wilson model. Each run was performed at a different setting of the I_{dc} injected current, with stimulation values ranging from -10.0 to $+7.77$ $\mu A/cm^2$. For each realization, the maximum and minimum instantaneous voltages detected during the 200-ms experiment were recorded and plotted as a gray vertical line whose end points, δV^+ and δV^-, indicate the largest positive and largest negative deviations away from the I_{dc}-determined V^o steady state: $\delta V^+ = (V_{max} - V^o)$, and $\delta V^- = (V_{min} - V^o)$. Superimposed in black are the theoretical $\pm 3\sigma$ curves, indicating the three-standard-deviation limits of the probability density function for the noise-induced membrane voltage fluctuations, where the standard deviation is computed from Eq. (11) as $\sigma = \sqrt{\Sigma_{11}}$.

The expected growth in voltage fluctuations is clearly evident in Fig. 6(a) as a yawning cornucopia that widens abruptly as stimulus current approaches the critical value $I_{dc}^{crit} \approx 7.77327$ $\mu A/cm^2$. The agreement between nonlinear simulation (gray) and Ornstein-Uhlenbeck theory (black) is very gratifying, although we note that a fairer test might have been to run *longer* simulations when the injected current is close to the I_{dc}^{crit} threshold in order to better capture the large deviations that occur on increasingly slowed time scales. We should also note that, towards the extreme right of the graph, the elevated membrane sensitivity sometimes resulted in the formation of one or more full-scale spikes, causing extremely large deviations—about two orders of magnitude larger than the scale of the graph. Clearly the linear theory is *not* applicable for such spike events. Notwithstanding these "outliers," provided the membrane remains in its subthreshold regime, linear Ornstein-Uhlenbeck theory works well.

From Eqs. (27) and (28), we expect the squid-membrane fluctuations to exhibit increasing spectral coloration or "ringing" as I_{dc} approaches threshold. This trend towards increasingly narrow resonances at $\omega_o/2\pi \approx \pm 360$ Hz is illustrated in the family of double-sided spectral-amplitude curves for $\tilde{v}_{rms} = \sqrt{S_{11}}$ plotted in Fig. 6(b). (Note that the actual spiking frequency of ~ 175 s^{-1} [see top trace of Fig. 1(a)] that emerges once threshold has been crossed is not well-estimated from our small-fluctuations linear theory—this is because spiking is a gross, highly nonlinear dynamical behavior.)

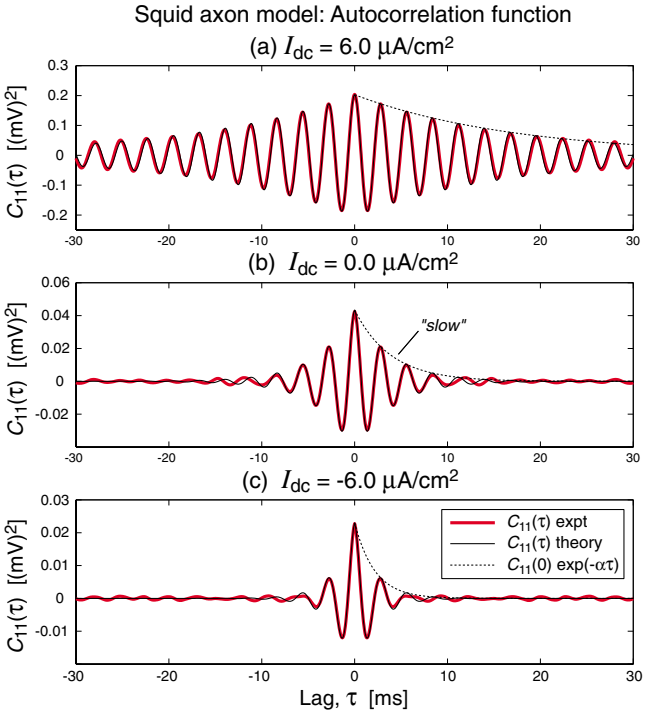

FIG. 7. (Color online) Autocorrelation graphs for white-noise-driven subthreshold squid axon (resonator) model at three levels of I_{dc} injected current: (a) 6.0; (b) 0.0; and (c) -6.0 $\mu A/cm^2$. Black curves show the $C_{11}(\tau)$ Ornstein-Uhlenbeck predictions; the thick-red curves show numerical results computed from the average of three independent 1000-ms stochastic simulation runs for each value of I_{dc}. The dashed curve labeled "slow" is the decay envelope $\exp(-\alpha\tau)$, where $\alpha = -\mathrm{Re}(\lambda_{1,2})$, predicted from the real part of the eigenvalue for the linearized squid axon. Consistent with the *noise-free* impulse runs of Fig. 2, the "slow" time-constant $T_{slow} = 1/\alpha$ diverges towards infinity as the stimulation current increases towards the threshold value $I_{dc}^{crit} \approx 7.77327$ $\mu A/cm^2$. The simulation time step is $\Delta t = 0.05$ ms.

Rather than comparing the Fig. 6(b) ideal squid spectra against an experimental estimate derived from many averaged Fourier transforms of the simulation time series, we have opted instead to gather the equivalent information in the time-domain via the autocorrelation function. See Fig. 7.

We selected three levels of injected current, and, for each level, ran three 1000-ms nonlinear stochastic simulations of the Wilson squid equations, then computed the autocorrelation function for the time series of the *zero-mean* voltage fluctuations (i.e., deviations about equilibrium). The curves displayed in bold red (colored gray in print version) are the three-run averages obtained using MATLAB's xcorr() function, and the thin-black curves are the $C_{11}(\tau)$ theoretical autocorrelation predictions [see Eqs. (20) and (23)]. The dashed curve shows the $\exp(-\alpha\tau)$ decay envelope predicted by the real part of the squid eigenvalue, $\alpha = -\mathrm{Re}(\lambda_{1,2})$. The match

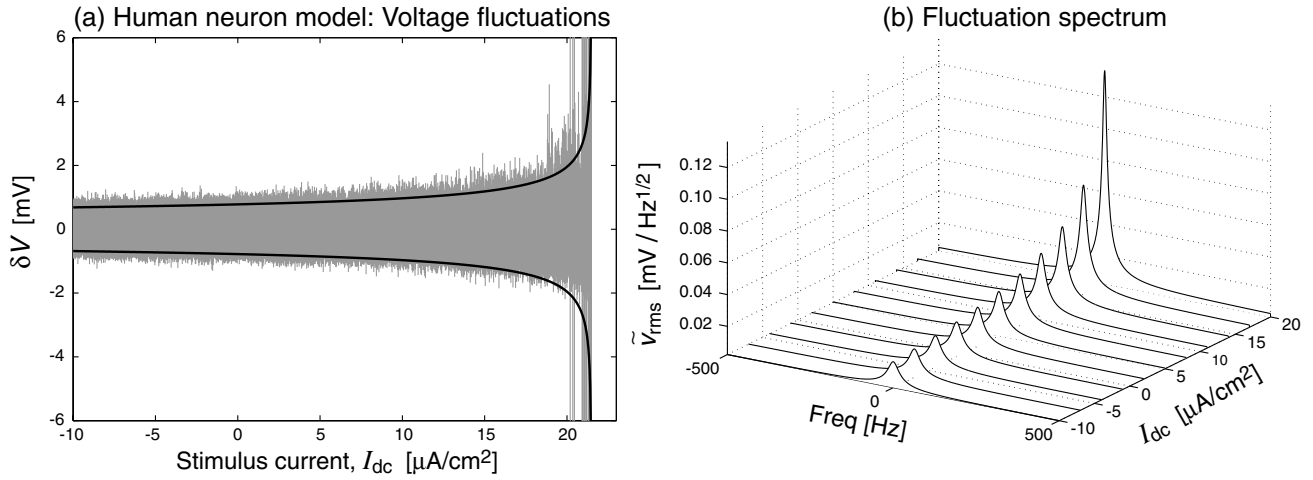

FIG. 8. Model cortical-neuron subthreshold response to white-noise perturbation as a function of stimulus current. (a) Caption as for Fig. 6(a), but with stimulus current for cortical neuron ranging from −10.0 to +21.475 μA/cm^2. Black curves are $\pm 3\sigma$ predictions; gray background verticals indicate fluctuation extrema recorded from 2000 independent numerical experiments. (b) The theoretical spectrum for subthreshold cortical neuron shows a strong resonance developing at zero frequency as threshold current for spiking is approached from below.

between theory and experiment is excellent, and we conclude that the subthreshold Wilson squid model behaves like a narrow-band damped oscillator whose damping diminishes towards zero as I_{dc} approaches spiking threshold.

B. Cortical-neuron stochastic response

Figures 8 and 9 are the cortical-neuron response curves corresponding to the squid-axon curves of Figs. 6 and 7. Figure 8(a) summarizes the voltage fluctuation extrema registered during 2000 independent stochastic trials of the Wilson cortical neuron, each trial lasting 200 ms, and stimulated at one of 2000 levels of injected dc current ranging from −10.0 to +21.475 μA/cm^2. The increased susceptibility of the neuron to white-noise perturbations is clearly evident as I_{dc} approaches the critical value $I_{dc}^{crit} \approx 21.4752$ μA/cm^2, and is well-matched by the divergent $\pm 3\sigma$ theoretical trend lines predicted from Eqs. (11) and (12). Here, $\sigma \equiv \sqrt{\Sigma_{11}} = \sqrt{\mathrm{var}\{v\}}$.

The Fig. 8(b) theoretical spectra from Eq. (25) for the cortical neuron fluctuations show a nearness-to-threshold sensitivity that is very similar to that seen in the squid axon [Fig. 6(b)], apart from the significant fact that the location of the resonance pole is now at *zero* frequency. This leads to the provocative idea that a type-I integrator membrane can be thought of as a type-II resonator that "resonates" at dc.

The autocorrelation graphs (Fig. 9, thick red curves) derived from nonlinear simulations of the Wilson cortical neuron agree nicely with the Ornstein-Uhlenbeck predictions of Eqs. (20) and (22) (black curves), but considerable care and attention to detail were required to secure this agreement. (See Appendix A and Table III for technical details.) Both sets of curves show a rapidly decaying "needle" riding on a much more slowly decaying "shoulder." These two features are set by λ_2 (the more negative eigenvalue) and λ_1 (the dominant, less negative eigenvalue), respectively. As the injected current approaches spiking threshold [panels (c) → (b) → (a)], the autocorrelation becomes dominated by the shoulder, rising in amplitude by ~three orders of magnitude, and becoming much more nearly horizontal as the T_{slow} correlation time increases from 10.8 ms [panel (c)] to 96.2 ms [panel (a)]. The trend towards a critically slowed, infinitely persistent autocorrelation function at the $I_{dc} \to I_{dc}^{crit}$ limit is clear. At this unreachable extremum, the autocorrelation is pure dc, consistent with its Fourier transform being a delta-function at zero frequency.

V. CONCLUSIONS AND DISCUSSION

In this paper we have offered a careful analysis of the subthreshold (nonspiking) behavior of a pair of biophysically motivated excitable membrane models developed by H. R. Wilson: the squid axon, a type-II "resonator;" and the human cortical neuron, a type-I "integrator." We have shown that these two membrane types display very distinctive voltage impulse responses when driven towards spiking threshold by a staircase-shaped injection current. For the squid model, the rising edge of each current step provokes a ringing voltage

TABLE III. Cortical (integrator) neuron time scales and numerical simulation settings for the three autocorrelation graphs shown in Fig. 9. The "noise attenuation" entries are the scale divisors applied to the variances of the two white-noise sources *prior* to simulation, then applied afterwards as compensatory multipliers to the experimentally determined autocorrelation measurements.

Value	Figure 9(c)	Figure 9(b)	Figure 9(a)	Unit
Stimulus, I_{dc}	0.0	20.0	21.4	μA/cm^2
Predicted T_{slow}	10.8	26.3	96.2	ms
Predicted T_{fast}	0.079	0.14	0.18	ms
Time step, Δt	0.02	0.05	0.05	ms
Integration time	1000	4000	10 000	ms
Noise attenuation	1	100	1000	

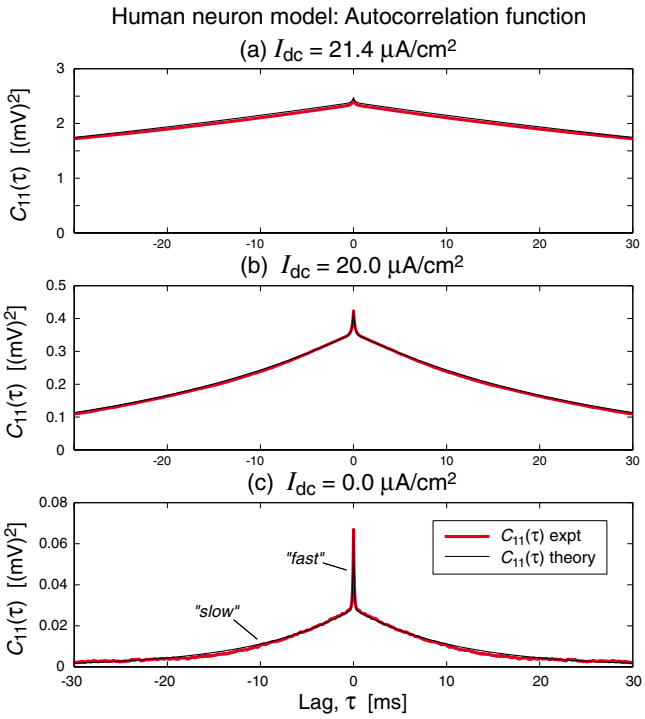

FIG. 9. (Color online) Autocorrelation graphs for white-noise-driven subthreshold cortical neuron (integrator) model at three levels of I_{dc} injected current: (a) 21.4; (b) 20.0; and (c) 0.0 $\mu A/cm^2$. Black curves show $C_{11}(\tau)$ theoretical predictions; background thick gray (online: thick red) curves show autocorrelation results averaged across three nonlinear stochastic simulation runs. As seen in the noise-free impulse responses in Fig. 3, there is an initial fast-decaying "needle" that rides on a much more slowly decaying exponential "shoulder" whose slope becomes more nearly horizontal as I_{dc} approaches threshold. Although the graphs show excellent agreement between Ornstein-Ulenbeck prediction and nonlinear numerics, securing this agreement is technically challenging, particularly for graph (a) where the stimulation current is set very close to threshold—see Appendix A and Table III for further details.

overshoot whose amplitude and persistence increase nonlinearly as the current approaches threshold. In contrast, the cortical neuron tends to smoothly integrate each step change in stimulus current, with a response time that becomes ever slower as the stimulus approaches threshold. In both cases, it is the altering eigenvalue structure that is causing the dramatic prolongation ("critical slowing") of response time, with infinite response times predicted when the dominant eigenvalue (or, for the type-II membrane, when the real part of the eigenvalue pair) touches zero.

These impulse properties are preserved when the staircase stimulus current is replaced by low-level white noise superimposed onto a constant level of injected current, I_{dc}. By linearizing about a given I_{dc}-determined subthreshold equilibrium point, we reformulated the stochasticized Wilson equations into a two-dimensional Ornstein-Uhlenbeck process, and were then able to write down exact analytic expressions for the noise-induced fluctuation variance, autocorrelation, and spectrum, and to deduce scaling laws for the divergences in correlation time and white-noise susceptibility. We demonstrated excellent agreement between the predicted fluctuation statistics and those measured from a series of stochastic simulations of the Wilson equations.

Given that spike generation is an inherently nonlinear process, is it reasonable to expect a linear theory to give good results for a noise-driven subthreshold neuron that is arbitrarily close to spiking threshold? After performing a large number of stochastic trials for the H. R. Wilson mammalian neuron sitting just below threshold, we have found that, provided the noise is sufficiently small, linear theory works well. However, for moderate noise levels, the nonlinear terms tend to grow, eventually swamping the linear terms and leading inexorably to the generation of a spike. (See Appendix B for details of the full Taylor-series analysis of the Wilson mammalian neuron.) We conclude that linear theory is appropriate for small subthreshold fluctuations; when fluctuations become sufficiently large that the nonlinear effects become significant, the neuron is about to change state from small-scale local stochastics to gross-scale nonlinear limit-cycle dynamics.

We see no reason why the critical slowing ideas reported here could not be tested in a neurophysiological laboratory that is equipped to measure the membrane voltage of a current-clamped neuron. The nonstandard aspect would be the requirement for white-noise to be added to the dc current—although this may not be necessary if there is sufficient "biological" background noise present in the cell. For a constant level of white-noise perturbation, we would expect to see nonlinear increases in correlation time and susceptibility (cell responsiveness) as the threshold point for firing is approached.

These findings may have biophysical significance. The slowed voltage fluctuations generated by an integrator neuron near threshold could "recruit" nearby neurons—possibly via the continuous diffusive coupling afforded by electrical gap junctions [38]—leading to population-wide subthreshold fluctuations that are correlated in time and space. Such correlated fluctuations would increase the likelihood that a spontaneous spike generated by one neuron could elicit a cascade of synchronized action potentials in its diffusively coupled neighbors. An anonymous referee has pointed out that the successful recruitment of prepared neighbors may require very fine tuning of both noise intensity and nearness to threshold—requirements that may turn out to be biologically unrealistic. Notwithstanding this caveat, if our ideas are correct, then neurons might be capable of accessing two quite distinct communication channels: a subtle subthreshold analog communication channel (via gap junctions) prior to firing, and a pulsed binary channel (via chemical synapses) once the neuron has crossed firing threshold.

APPENDIX A: SIMULATION OF AN INTEGRATOR NEURON CLOSE TO THRESHOLD

Our Ornstein-Uhlenbeck treatment for subthreshold excitable membranes is only valid when the voltage and recovery-variable fluctuations—resulting from white-noise perturbations—are sufficiently small that the contributions from the nonlinear terms in Eqs. (1) are negligible. If the fluctuations grow to the point that the neuron crosses thresh-

old, then its behavior abruptly switches over from small-scale subthreshold *linear stochastics* to gross-scale suprathreshold *nonlinear dynamics*: the neuron fires an action-potential spike. Therefore, in stochastic numerical simulations designed to test the linear theory, we require that the neuron remain in its subthreshold regime, and never generate a spike. However, because the responsiveness (susceptibility) of the subthreshold membrane scales inversely with the dominant eigenvalue, λ_1 (or, for the resonator neuron, inversely with the real part of the eigenvalue), close-to-threshold numerical experiments are particularly challenging. Not only does $1/\lambda_1$ determine the subthreshold "gain," it also defines the slow time scale over which the response will persist, and both of these quantities will diverge as $\lambda_1 \to 0$.

Consequently, a successful close-to-threshold stochastic simulation requires that the following conditions be simultaneously satisfied.

1. The noise stimulation must be sufficiently small that the neuron does not cross threshold and generate a spike.

2. The experiment must run for sufficient time to capture the slow dynamics with good fidelity.

3. The time step Δt must be fine enough to capture the fast dynamics set by the second eigenvalue.

In practice, we have found that condition 1 requires that the noise amplitude be dramatically scaled down for experiments near threshold. For condition 2, a rule-of-thumb for accurate slow dynamics is that the simulation be run for a time $T \gtrsim 100 T_{\text{slow}}$, where $T_{\text{slow}} = -1/\lambda_1$. Condition 3 leads to a Nyquist-like criterion for setting the sampling interval: $\Delta t \lesssim \frac{1}{2} T_{\text{fast}}$, where $T_{\text{fast}} = -1/\lambda_2$. [For the resonator membrane, $T_{\text{slow}} = -1/\text{Re}(\lambda_{1,2})$, and $T_{\text{fast}} = 2\pi/|\text{Im}(\lambda_{1,2})|$ is the period of subthreshold oscillations.]

Table III summarizes the simulation settings used to generate the three integrator-neuron autocorrelation plots shown in red (gray in print version) in Fig. 9. As the dc stimulus current was increased from 0.0 [Fig. 9(c)] to 21.4 $\mu\text{A/cm}^2$ [Fig. 9(a)], the experiment duration was increased by an order of magnitude to cater for the predicted $\sim \times 10$ dilation of the T_{slow} time scale, while the intensity (variance) of the white-noise sources was scaled down by a factor of 1000 to reduce the chance of spike generation. The measured autocorrelation statistic was subsequently scaled up by the same factor to allow comparison with the default noise intensities used for the $I_{\text{dc}} = 0$ run.

APPENDIX B: TAYLOR-SERIES ANALYSIS FOR MAMMALIAN NEURON

The noise-free form of the Wilson mammalian neuron is given in Eq. (4); explicit polynomial expressions for sodium conductance $g_{\text{Na}}(V)$ and recovery steady state $G(V)$ are listed in Table I. Since we are interested in the (v,r) fluctuations about a nominated steady state $(V^{\text{o}},R^{\text{o}})$, we write $(V,R) = (V^{\text{o}}+v, R^{\text{o}}+r)$, and make a two-variable Taylor expansion about this steady state,

$$F_{1,2}(V,R) = F_{1,2}(V^{\text{o}},R^{\text{o}}) + v \left.\frac{\partial F_{1,2}}{\partial V}\right|_{\text{o}} + r \left.\frac{\partial F_{1,2}}{\partial R}\right|_{\text{o}} + \frac{1}{2}v^2 \left.\frac{\partial^2}{\partial V^2}F_{1,2}\right|_{\text{o}} + vr \left.\frac{\partial^2}{\partial V \partial R}F_{1,2}\right|_{\text{o}} + \frac{1}{2}r^2 \left.\frac{\partial^2}{\partial R^2}F_{1,2}\right|_{\text{o}} + \frac{1}{6}v^3 \left.\frac{\partial^3}{\partial V^3}F_{1,2}\right|_{\text{o}} + \cdots, \tag{B1}$$

where all partial derivatives are evaluated at the $(V^{\text{o}},R^{\text{o}})$ steady state, and $F_1(V^{\text{o}},R^{\text{o}}) = F_2(V^{\text{o}},R^{\text{o}}) = 0$. Because F_1 is a cubic polynomial in V, and F_2 is a quadratic polynomial in V, the higher-order terms denoted $(\cdots)$ are all zero. Therefore this Taylor expansion is *exact* for all values of (v,r), and, in particular, there is no requirement here that the (v,r) fluctuations be small.

Evaluating Eq. (B1) and simplifying, we obtain a pair of coupled equations for the membrane voltage and recovery fluctuations whose form allows us to identify clearly the linear and nonlinear contributions to the motion,

$$\frac{dv}{dt} = J_{11}v + J_{12}r + k_1 v^2 + k_2 vr + k_3 v^3, \tag{B2a}$$

$$\frac{dr}{dt} = J_{21}v + J_{22}r + \ell_1 v^2. \tag{B2b}$$

The four J_{mn} coefficients are the elements of the Jacobian matrix evaluated at the equilibrium point. The coefficients for the nonlinear terms are

$$k_1 = [-a_2(3V^{\text{o}} - E_{\text{Na}}) - a_1]/C,$$

$$k_2 = -26/C,$$

$$k_3 = -a_2/C,$$

$$\ell_1 = b_2/\tau_R,$$

where $a_1 = 47.58$, $a_2 = 33.8$, $b_2 = 3.30$, $E_{\text{Na}} = 0.48$, $C = 1.0$, and $\tau_R = 5.6$ (see Table I for units). The k_1 constant is positive. For large fluctuations, $dv/dt \approx k_1 v^2$, and the voltage perturbation will grow *faster than exponentially* (in fact, the growth will be hyperbolic—see Gerstner and Kistler's description of the quadratic integrate-and-fire neuron on p. 99 of Ref. [8]). The v^2 nonlinearity is the primary driver for spike initiation in this model. The $k_3 v^3$ term cuts in later and more steeply, but, because it is negative, it acts as a delayed restoring force to cancel the hyperbolic divergence of the $k_1 v^2$ term. The $k_2 vr$ term is the nonlinear coupling responsible for speeding and shaping the down-stroke of the spike.

Since the selected equilibrium point is stable, all four Jacobian elements are negative. If the nonlinear terms v^2, vr, v^3 are negligible, then the linear terms will drive an exponential decay to steady state on time scales T_{slow} and T_{fast} determined by λ_1 and λ_2, the dominant and second eigenvalues of the Jacobian matrix: $T_{\text{slow}} = 1/|\lambda_1|$, $T_{\text{fast}} = 1/|\lambda_2|$. For example, setting the stimulus current to $I_{\text{dc}} = 0.214\,752\,886\,070\,6788$ (in units $10^2\ \mu\text{A/cm}^2$) renders a stable bottom-branch steady state that is exceedingly close to

the saddle-node annihilation point. At this location, the time scales are $T_{\text{fast}} \approx 0.196$ ms and $T_{\text{slow}} \approx 28.363 \times 10^6$ ms ≈ 7.9 h(!). According to the guidelines established in Appendix A, one would need to simulate a ~790-h or ~1-month interval at ~0.05-ms resolution in order to adequately capture the full extent of the critically slowed fluctuation statistics.

We wished to establish the relative importance of the linear and nonlinear terms of Eqs. (B2), particularly for a neuron very close to threshold, so we ran a large number of stochastic simulations with dc current settings ranging up to and including the precise 16-digit value listed in the previous paragraph. For moderate levels of noise, the fluctuations rapidly became large, with growth of the nonlinear terms swamping the linear relaxation, leading to the prompt generation of an action potential.

Spike onset could be delayed by scaling back the noise, making it possible to examine in "slow motion" the prelude to spike formation. It became clear that as soon as the nonlinear contributions to the rate-of-change became comparable to the linear contributions, subsequent generation of a spike was almost inevitable: the nonlinear terms destabilize the equilibrium, while the linear terms stabilize it.

We conclude that a noise-driven subthreshold Wilson neuron can only remain subthreshold when the fluctuations remain sufficiently small that the nonlinear contributions are negligible. It is for this reason that the linear Ornstein-Uhlenbeck analysis presented in this paper provides an accurate description of the subthreshold neuron: the stochastic resting neuron is linear; the dynamic spiking neuron is nonlinear.

[1] Z. F. Mainen and T. J. Sejnowski, Science **268**, 1503 (1995).
[2] E. Schneidman, B. Freedman, and I. Segev, Neural Comput. **10**, 1679 (1998).
[3] B. S. Gutkin and G. B. Ermentrout, Neural Comput. **10**, 1047 (1998).
[4] R. Guantes and G. G. de Polavieja, Phys. Rev. E **71**, 011911 (2005).
[5] L. Gammaitoni, P. Hanggi, P. Jung, and F. Marchesoni, Rev. Mod. Phys. **70**, 223 (1998).
[6] R. K. Adair, Proc. Natl. Acad. Sci. U.S.A. **100**, 12099 (2003).
[7] R. C. Hilborn, Am. J. Phys. **72**, 528 (2003).
[8] W. Gerstner and W. Kistler, *Spiking Neuron Models: Single Neurons, Populations, Plasticity* (Cambridge University Press, Cambridge, England, 2002).
[9] A. Longtin, Phys. Rev. E **55**, 868 (1997).
[10] R. C. Hilborn and R. J. Erwin, Phys. Rev. E **72**, 031112 (2005).
[11] R. Dermietzel, Brain Res. Rev. **26**, 176 (1998).
[12] M. Galarretta and S. Hestrin, Nat. Rev. Neurosci. **2**, 425 (2001).
[13] M. V. Bennett and R. S. Zukin, Neuron **41**, 495 (2004).
[14] M. Galarretta and S. Hestrin, Nature (London) **402**, 72 (1999).
[15] Y. Amitai *et al.*, Int. J. Neural Syst. **22**, 4142 (2002).
[16] S. R. Hameroff, Anesthesiology **105**, 400 (2006).
[17] J. Rinzel and G. B. Ermentrout, in *Methods in Neuronal Modeling*, edited by C. Koch and I. Segev (MIT Press, Cambridge, MA, 1989), pp. 135–169.
[18] S. H. Strogatz, *Nonlinear Dynamics and Chaos* (Westview Press, Cambridge, MA, 2000).
[19] E. M. Izhikevich, Int. J. Bifurcation Chaos Appl. Sci. Eng. **10**, 1171 (2000).
[20] C. W. Gardiner, *Handbook of Stochastic Methods for Physics, Chemistry, and the Natural Sciences*, Vol. 13 of Springer Series in Synergetics, 3rd ed. (Springer-Verlag, Berlin, 2004).
[21] A. L. Hodgkin, J. Physiol. (London) **107**, 165 (1948).
[22] A. Manwani and C. Koch, Neural Comput. **11**, 1797 (1999).
[23] I. A. Fleidervish, C. Gebhardt, N. Astman, M. J. Gutnick, and U. Heinemann, Int. J. Neural Syst. **21**, 4600 (2001).
[24] H. R. Wilson, *Spikes, Decisions and Actions: The Dynamical Foundations of Neuroscience* (Oxford University Press, New York, 1999).
[25] M. L. Steyn-Ross, D. A. Steyn-Ross, J. W. Sleigh, and D. T. J. Liley, Phys. Rev. E **60**, 7299 (1999).
[26] M. L. Steyn-Ross, D. A. Steyn-Ross, J. W. Sleigh, and L. C. Wilcocks, Phys. Rev. E **64**, 011917 (2001).
[27] M. L. Steyn-Ross, D. A. Steyn-Ross, J. W. Sleigh, and D. R. Whiting, Phys. Rev. E **68**, 021902 (2003).
[28] M. L. Steyn-Ross, D. A. Steyn-Ross, and J. W. Sleigh, Prog. Biophys. Mol. Biol. **85**, 369 (2004).
[29] D. A. Steyn-Ross, M. L. Steyn-Ross, J. W. Sleigh, M. T. Wilson, I. P. Gillies, and J. J. Wright, J. Biol. Phys. **31**, 547 (2005).
[30] M. L. Steyn-Ross, D. A. Steyn-Ross, J. W. Sleigh, M. T. Wilson, and L. C. Wilcocks, Phys. Rev. E **72**, 061910 (2005).
[31] M. T. Wilson, M. L. Steyn-Ross, D. A. Steyn-Ross, and J. W. Sleigh, Phys. Rev. E **72**, 051910 (2005).
[32] J. Rinzel, Fed. Proc. **44**, 2944 (1985).
[33] A. L. Hodgkin and A. F. Huxley, J. Physiol. (London) **117**, 500 (1952).
[34] R. FitzHugh, Biophys. J. **1**, 445 (1961).
[35] J. S. Nagumo, S. Arimoto, and S. Yoshizawa, Proc. IRE **50**, 2061 (1962).
[36] H. Carmichael, *Statistical Methods in Quantum Optics: Master Equations and Fokker-Planck Equations* (Springer, Berlin, 1999).
[37] D. M. Wiberg, *State Space and Linear Systems*, *Schaum's Outline Series* (McGraw-Hill, New York, 1971).
[38] P. Balenzuela and J. Garcìa-Ojalvo, Phys. Rev. E **72**, 021901 (2005).
[39] P. E. Kloeden and E. Platen, *Numerical Solution of Stochastic Differential Equations* (Springer, Berlin, 1992).
[40] Locating the isocline intersection points for the Wilson type-I neuron involves finding the roots in a *cubic* polynomial in membrane voltage, so the lower-right saddle-node turning point marks the annihilation of exactly *two* roots; therefore the local curvature cannot be higher-order than quadratic.